

Article

Simple and Rapid Preparation of MIL-121 with Small Particles for Lithium Adsorption from Brine

Qinyan Wei, Bingqian Shi, Fei Wang, Shuoshuo Shao, Liang Zhu * and Xiaoyu Zhao *

College of Chemical Engineering and Materials Science, Tianjin University of Science & Technology, Tianjin 300457, China; weiqy@mail.tust.edu.cn (Q.W.); shibq@mail.tust.edu.cn (B.S.); yifei@mail.tust.edu.cn (F.W.); woshihuaidan83@mail.tust.edu.cn (S.S.)

* Correspondence: zhuliang@tust.edu.cn (L.Z.); xyz@tust.edu.cn (X.Z.)

Abstract: A novel method to generate an aluminum-based MOF material named as MIL-121 was investigated. MIL-121, $[\text{Al}(\text{OH})(\text{H}_2\text{BTEC})\cdot(\text{H}_2\text{O})]_n$ is a prototypal aluminum MOF with 1,2,4,5-benzenetetracarboxylic acid (BTEC) linkers, which was normally produced by the hydrothermal method. Different from the hydrothermal method, the developed novel method does not involve high temperature and high pressure, instead the MOF material was produced by the traditional cooling crystallization method at ambient pressure and low temperature below 100 °C. The MIL-121 obtained by the novel method possesses the same lithium adsorption performance as that obtained by hydrothermal method, but with lower energy consumption and more environmentally friendly. Compared with hydrothermal method, this method has more advantage to be scaled up to industrialized production. The formation mechanism of MIL-121 in the novel method including nucleation and growth process of MOF crystal was studied. The results indicated that the size and morphology of MIL-121 crystals were influenced by the temperature and additives, respectively. As the reaction temperature increased to 100 °C, the operation time can be shortened to 2–5 h. The crystal habit that was predicted by Material studio software using BFDH, which is a model for crystal habit prediction proposed by Bravais, Friedel, Donnay, and Harker based on the crystal lattice parameters and crystal symmetry in the Morphology module, the simulated morphology of MIL-121 was in accord with that of the products obtained by cooling crystallization. The thermal stability of MIL-121 obtained by cooling crystallization is better than that obtained by the hydrothermal method.

Keywords: ambient pressure; adsorption; cooling crystallization; particle size; thermal stability; industrialization



Citation: Wei, Q.; Shi, B.; Wang, F.; Shao, S.; Zhu, L.; Zhao, X. Simple and Rapid Preparation of MIL-121 with Small Particles for Lithium Adsorption from Brine. *Coatings* **2021**, *11*, 854. <https://doi.org/10.3390/coatings11070854>

Academic Editor: Mazeyar Parvinzadeh Gashti

Received: 29 May 2021

Accepted: 8 July 2021

Published: 16 July 2021

Publisher's Note: MDPI stays neutral with regard to jurisdictional claims in published maps and institutional affiliations.



Copyright: © 2021 by the authors. Licensee MDPI, Basel, Switzerland. This article is an open access article distributed under the terms and conditions of the Creative Commons Attribution (CC BY) license (<https://creativecommons.org/licenses/by/4.0/>).

1. Introduction

About 59% of the global lithium resources exist in salt lake brines [1]. The salt lake brines are rich in water resources and the lithium extraction process is simple and low in cost [1]. The selection factors of the method of extracting lithium from salt lake brine mainly include the concentration of brine lithium and the content of the main components (such as Na^+ , K^+ , Ca^{2+} , Mg^{2+} , Cl^- , SO_4^{2-} , CO_3^{2-} , etc.), brine salinity, and process route technology possibility, economic feasibility, and local characteristics of the salt lake. The currently developed methods for extracting lithium from salt lake brine include adsorption method [2], membrane separation method [3], precipitation method [1,4], electrochemical method [5–8], reaction-coupling separation technology [9,10], solvent extraction method [11,12], and so on. Among the many methods mentioned above, the adsorption method has great advantages in terms of economy and environmental protection for extracting lithium from brine with a high magnesium-to-lithium ratio and low lithium concentration. Its process is relatively simple, with low energy consumption, high recovery rate, and good selectivity, which is an optimal process scheme [2,13].

Commonly used adsorbents mainly include aluminum salt adsorbents, lithium-ion sieves, and nanofiltration membranes [14,15]. Kotsupalo [14] et al. studied $\text{LiCl}\cdot 2\text{Al}(\text{OH})_3\cdot \text{mH}_2\text{O}$

adsorbent for extracting lithium from brine with a high Mg/Li ratio, with an adsorption capacity of about 7–8 mg/g. Even if the brine contains a high concentration of MgCl_2 , the adsorbent has a good selectivity to lithium. Increasing the concentration of MgCl_2 from 0–500 g gradually increases the lithium adsorption capacity by nearly four times. Tian et al. [13] prepared $\text{LiMg}_{0.56}\text{Mn}_{1.5}\text{O}_4$ by a chemical method, and the lithium extraction performance was greater than 95% after five recycles. Chitrakar [16] found that by increasing the Mg/Mn ratio to increase the chemical stability of the ion sieve to improve the adsorption capacity of Li^+ , the manganese loss rate was less than 0.25 wt%. In addition, magnesium doping accelerates the adsorption equilibrium and improves the lithium recovery efficiency. Bi et al. [17] studied the application of 3B02S nanofiltration membrane for lithium extraction from brine, and the results showed that the membrane has a good exclusion of Mg^{2+} and achieved the recovery of lithium from brine with a high Mg/Li ratio.

The modified PDMVBA-MIL-121 was used as a renewable metal salt ion adsorbent [18] and A-MIL-121 was used in the renewable adsorption of heavy metal ions [19]. However, the only method for the synthesis of MIL-121 that has been reported is the hydrothermal method. The hydrothermal method requires reaction at high temperature above 180 °C for about 24–48 h [18]. As the widespread application of MIL-121, it is urgent to develop a green and stable efficient production process.

It is evident that metal-organic framework nanoparticles (nano MOFs) have superior performance compared to their bodies. However, little knowledge is known about the relationship between hydrothermal synthesis conditions and MOF particle size. The influence of temperature and $[\text{2-MeIM}]/[\text{Zn}^{2+}]$ ratio on the synthesized ZIF-8 nanoparticles was systematically investigated by Yamamoto et al. [20]. It is concluded that lower temperature and higher $[\text{2-MeIM}]/[\text{Zn}^{2+}]$ ratio are crucial conditions for the preparation of small-sized ZIF-8 nanoparticles. Lowering the hydrothermal reaction temperature will increase the number of nuclei and give rise to the generation of smaller nanoparticles. Marshall et al. proposed a seesaw model according to the summary of the nanocrystal model, which described the formation of nanocrystals as a kinetic competition between acid-base reaction and metal ligand reactivity [21]. The relative influence of the reaction parameters such as solution acidity, ligand excess, and reactant concentration on the particle size of nanoparticles has been verified by experiments. However, this model does not fit all systems. For some specific MOF systems, it is essential to investigate the particle size control methods by experiments.

In addition, the synthesis of MOF with high thermal stability has become the focus of many investigators [22]. Most of the currently reported high-stability MOFs were prepared by hydrothermal methods, which have high synthesis costs, harsh reaction conditions, and excessive use of toxic organic solvents [23–25]. Although MOFs have been applied in the preparation of new materials such as drug carriers, composite membranes, nanoreactors, luminescence sensors, dielectric materials, capacitors, etc., [26–32], there are only a few of them which have been applied to the actual production process. Optimization and amplification of the MOF synthesis process are still extremely challenging, which has brought major obstacles to the synthesis and realization of many other promising MOF structures [33]. Achieving the mass production and widespread use of MOFs, it is inevitable to develop green and environmentally friendly synthetic methods. Studies have reported that milder reaction conditions, greener metal nodes, and sources of organic ligands are the top priority for the green synthesis of MOFs [34]. Much progress has been made on hydrothermal methods [35]. However, there is a basic requirement for hydrothermal synthesis. The reaction materials and products of hydrothermal synthesis must be of considerable thermal and chemical stability. In addition, operation of reaction at high temperature and high pressure leads to high energy costs and great risk of safety. In comparison, the ultrasonic hydrothermal method and mechanochemical hydrothermal method have the advantages of high efficiency and are environmentally friendly, but it is difficult to scale up [36–39]. Up to now, only BASF-SE company has achieved ton-scale

production of Basolite A520 material, which proved the difficulty to manufacture MOF material with hydrothermal method in [40].

In this article, a novel method to generate MIL-121 was investigated. The developed method can be used to produce MOF material at ambient pressure and temperature below 100 °C. The MIL-121 obtained by the novel method has the same lithium adsorption performance as that obtained by hydrothermal method, but with lower energy consumption and is more environmentally friendly. Compared to hydrothermal method, this method is more potential to be industrialized.

2. Materials and Methods

2.1. Material and Device

The parallel crystallizer (EasyMax 402 Basic, METTLER TOLEDO Group, Shanghai, China) produced by METTLER TOLEDO Group and the constant-speed program temperature controlled by a thermostat produced by Nanjing Xianou Instrument Co., Ltd. were used to control the cooling and crystallization process. The crystal products obtained in the experiments were observed by the field emission high-resolution scanning electron microscope SEM (FEI, Apreo, Japan). The powder X-ray diffractometer (Shimadzu XRD-6100, Shimadzu, Japan) and Fourier infrared spectrometer FTIR (BRUKER TENSOR 27, Bruker, Germany) provided by the Analysis Center of the School of Chemical Engineering and Materials were used for qualitative analysis of the products. The TG (Netzsch, Germany) was implemented to analyze the thermal stability of the crystal material in the temperature range of 50–800 °C under the protection of N₂ atmosphere. The LabRAM HR800 microprobe Raman system was used to analyze the Raman peak of the product. The particle size distribution of the crystals is also analyzed by the BECKMANCOULTER LS series laser particle size analyzer.

In order to confirm the crystal form and polymorphic purity of the products, powder X-ray diffraction (PXRD) patterns were recorded on a Shimadzu PXRD-6100 diffractometer equipped with Cu K α source at a scanning rate of 5° min⁻¹. The crystal habit of MIL-121 was determined by scanning electron microscope SEM (FEI, Apreo, Japan). The size of the crystals was characterized using a laser diffraction particle size analysis meter (Beckman Coulter LS, Beckman, CA, America) at a pump speed of 52 r/min and ultrasonic time 5 s. The Fourier transform-infrared (FT-IR) spectra (potassium bromide pellets) were obtained on a TENSOR27 (Bruker, Germany) FT-IR spectrometer instrument in the wavenumber range of 400–4000 cm⁻¹. The Raman detection was carried out on a LabRAM HR800 microprobe Raman system (Horiba Jobin-Yvon, France) with excitation of 532 nm. The Raman band of a silicon wafer at 520 cm⁻¹ was used as a reference to calibrate the spectrometer. The Raman shift range is 250–4000 cm⁻¹ and the exposure time is 5 s. The thermogravimetric data were collected by SDT-Q600 differential of American TA Company performed in the temperature range of 40–50 °C, with a temperature scanning rate of 20 °C min⁻¹ in 50 mL min⁻¹ N₂ gas flow.

2.2. Investigation of the Crystallization Process

A parallel crystallizer (EasyMax 402 Basic) was used to investigate the cooling crystallization process. Al(NO₃)₃·9H₂O 2.4 g, H₄BTEC(pyromellitic acid) 0.8 g, and 10 mL deionized water were added to six identical 20 mL capped test tubes. The experiment adopts different holding time (3, 5, 10 h) and cooling method (cooling rate 0.3 °C/min and rapid cooling method). The reaction temperature was 80 and 100 °C, respectively. When the reaction temperature is 80 °C, as the reaction time increases, the output of MIL-121 also increases. The reaction temperature is 3 h, the product of MIL-121 is 0.083 g, the reaction temperature is 5 h, the product of MIL-121 is 0.231 g, the reaction temperature is 10 h, and the product of MIL-121 is 0.486 g. The effects of holding time, cooling method, and reaction temperature on the grain size and yield of MIL-121 were investigated.

2.3. Synthesis of MIL-121 by Low-Temperature Hydrothermal Method

The metal salt $\text{Al}(\text{NO}_3)_3 \cdot 9\text{H}_2\text{O}$, 1.2 g) and solvent (deionized water, 10 mL) were added into a 100-mL high pressure autoclave. The synthesis reaction was carried out at 80 °C after adding excess ligand ($\text{Al}(\text{NO}_3)_3 \cdot 9\text{H}_2\text{O}:\text{H}_4\text{BTEC}:\text{H}_2\text{O}$ ratio is 2:4:174) and a certain amount (1 mL NaOH aqueous solution with concentration of 4 mol/L) of sodium hydroxide. The operation details of this method are described in the literature reported before [41].

2.4. The Influence of Synthesis Temperature on Particle Size and Stability of MOF Particle

About 2.4 g of $\text{Al}(\text{NO}_3)_3 \cdot 9\text{H}_2\text{O}$, 0.8 g of H_4BTEC , and 10 mL of deionized water ($\text{Al}(\text{NO}_3)_3 \cdot 9\text{H}_2\text{O}:\text{H}_4\text{BTEC}:\text{H}_2\text{O}$ ratio is 2:1:174) were added to 1 mL NaOH aqueous solution with concentration 4 mol/L to carry out the experiment (See Supplementary Materials Figures S1 and S2 for the experimental results of the sodium hydroxide addition amount). Experiments were performed at hydrothermal synthesis temperatures of 80, 90, and 100 °C, the reaction time was 48 h, and the cooling rate was 5 °C/h. White products obtained in the experiment of 80 and 90 °C were washed with methanol three times and then with deionized water several times until pH > 4. The synthesis product obtained at 100 °C was washed only with deionized water.

2.5. The Influence of NaOH on the Cooling Crystallization Process of MIL-121

Two experiments were carried out to investigate the influence of NaOH on the synthesis of MIL-121. Total of 2.4 g of $\text{Al}(\text{NO}_3)_3 \cdot 9\text{H}_2\text{O}$, 0.8 g of H_4BTEC , and 10 mL of deionized water were added into two 50 mL identical crystallizers respectively. The temperature of the crystallizers coupled with a magnetic agitation was raised to 80 °C by using a temperature-controlled tank to make the ligand completely dissolved. The experiments of group A were performed without addition of NaOH aqueous solution to the crystallizer, and experiments of group B were carried out by slowly adding 1 mL NaOH aqueous solution with concentration of 4 mol/L. The system was sealed at 80 °C for 12 h and then the heating was stopped and let it cool down naturally. Solution samples were taken using a pipette at the intervals of 1, 3, 5, 10, and 12 h respectively during the constant temperature process and then volatilized naturally in a fume hood. Raman analysis is performed after the complete volatilization of the solvent.

2.6. Cooling Crystallization Experiment

A scale 100 mL experiment was carried out with a parallel crystallizer. About 7.044 g of $\text{Al}(\text{NO}_3)_3 \cdot 9\text{H}_2\text{O}$, 2.134 g of H_4BTEC , and 30 mL of deionized water were taken in the No. 1 kettle. The kettle is heated to 80 °C and the pyromellitic acid is completely dissolved, and then 3 mL NaOH aqueous solution with concentration of 4 mol/L is slowly added to keep the temperature constant for 7 h. Subsequently, the temperature was reduced to 20 °C at a rate of 0.3 °C/min. After centrifugal cleaning, it was dried in an oven at 80 °C for 24 h. The mass of the MIL-121 product obtained is 1.284 g.

2.7. Adsorption Performance Test

About 0.05 g of the polymerized sample PDMVBA-MIL-121 was taken and dispersed in 10 mL of lithium chloride salt solution and stirred for 16 h, and then centrifuged for solid-liquid separation. Finally, a calibrated inductively coupled plasma spectrometer was used to measure the concentration of lithium ions in the supernatant after centrifugation. The standard solution for adsorption is a 10,000 ppm lithium chloride solution. The ICP test method is to use a pipette to take 1 mL of the solution to be tested in a 100 mL volumetric flask and dilute it with deionized water 100 times before testing the lithium-ion concentration.

3. Results

3.1. Morphology, Size, and Stability of Small Particle Size MIL-121

Figure 1 shows the PXRD of the small particle size MIL-121 obtained under different conditions in the Section 2.4. The samples obtained under the reaction temperatures of 80, 90, and 100 °C were named as MIL-121-80 °C, MIL-121-90 °C, and MIL-121-100 °C respectively. The position and intensity of the characteristic peaks of the PXRD patterns were all in line with the standard card of MIL-121 and previously reported pattern [42]. The structure of MIL-121 obtained by low-temperature hydrothermal method at 80 °C with excess ligand and sodium hydroxide was confirmed in the Section 2.3. The PXRD analysis result indicates that all the samples obtained under different reaction conditions have the same crystal form, which demonstrates that the addition of sodium hydroxide promoted the synthesis of MIL-121. With an increase in the reaction temperature from 80 °C to 100 °C, the intensity of PXRD characteristic peak increases. It indicated that the crystallinity is improved with an increase in reaction temperature. The crystal face index was obtained from the corresponding crystallographic information file of the PXRD data peak-fitting result (Table S1, Supplementary Materials). In addition, the infrared peaks and Raman peaks of the crystal products obtained under different synthesis conditions are the same (Figure S3a,b, Supplementary Materials), which means that the samples generated under different conditions are all MIL-121.

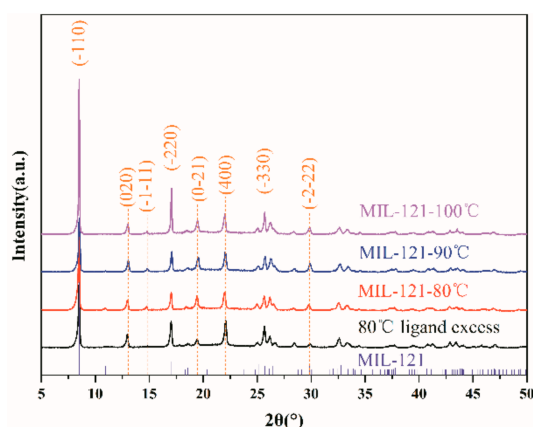


Figure 1. PXRD patterns of MIL-121-ligand excess, MIL-121-80 °C, MIL-121-90 °C, MIL-121-100 °C.

Figure 2a–d shows the SEM (Scanning electron microscopy) results for MIL-121 products under different reaction conditions. All products present the same morphology of regular polyhedron. The length to diameter ratio (LDR) of the products are slightly different. The LDR for the products crystallized under excessive ligands is less than 4, indicating the rapid growth of the $(\bar{1}\bar{1}1)$ crystal plane (Figure 2a,b). The products crystallized with the addition of sodium hydroxide have smooth surfaces, blunt edges, and complete appearance. From MIL-121-80 °C to MIL-121-100 °C, the length of the products increased from 1.2 μm to 3.5 μm . The particle size of MIL-121 was mainly affected by the synthesis temperature. In addition, the particle size of the product obtained with excess ligand at the synthesis temperature of 80 °C was smaller, but with lower yield about 10 mg. At the same synthesis condition, the yield was improved to 0.52 g by adding 1 mL NaOH aqueous solution with concentration of 4 mol/L. Obviously, sodium hydroxide accelerates the coordination reaction rate between the metal ion and the carboxylic acid ligand.

The average particle size, median particle size, and coefficient of variation of the product are shown in Table S2 (Supplementary Materials). With an increase in the hydrothermal synthesis temperature from 80 to 100 °C, D50 (median diameter) of the products increased from 2.15 to 3.94 μm . This was consistent with the SEM results. The coefficient of variation (C.V.) data confirmed that the particle size distribution has gradually widened with increased temperature. The particle size distribution of the product nearly conforms to a normal distribution (Figure S4, Supplementary Materials). The products crystallized

at different temperatures were of relatively high coefficient of variation, and the product distribution is relatively dispersed. As the synthesis temperature increases, the particle size of the product increases significantly.

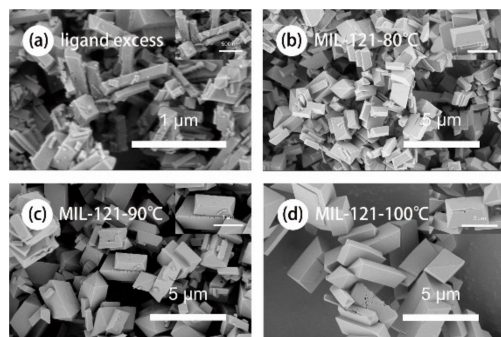


Figure 2. SEM images of (a) MIL-121-ligand excess, (b) MIL-121-80 °C, (c) MIL-121-90 °C, (d) MIL-121-100 °C.

In order to verify the stability of MIL-121-80 °C, MIL-121-90 °C, and MIL-121-100 °C under the auxiliary condition of sodium hydroxide, their thermal behaviors were characterized. Figure 3 shows their thermogravimetric (TG) curve. Table S4 (Supplementary Materials) shows the mass loss of MIL-121-80 °C, MIL-121-90 °C, and MIL-121-100 °C in thermogravimetric analysis. Through data comparison, it is found that the initial decomposition temperature of MIL-121-80 °C is 329 °C (the initial decomposition temperature is calculated with a mass loss of 10%). The initial decomposition temperatures of MIL-121-90 °C and MIL-121-100 °C are 357 and 375 °C (10%, mass loss), respectively. Their thermal behavior is manifested in three stages. The first stage is the removal of residual solvent and unreacted ligands in the MIL-121 channel. In the second stage of the framework decomposition begins. The free carboxyl groups on the MIL-121 framework are decomposed and converted into carbon dioxide. The third stage is mainly the conversion of the coordinated carboxyl groups on the MIL-121 framework to carbon dioxide and the rapid collapse and decomposition of the framework (Figure 3). When the decomposition is completed (800 °C), the remained mass fraction of MIL-121-80 °C is 27.6%, the remained mass fraction of MIL-121-90 °C is 34.5%, and the remained mass fraction of MIL-121-100 °C is 36.5%. It can be concluded that as the synthesis temperature increases, the thermal stability of the product increases.

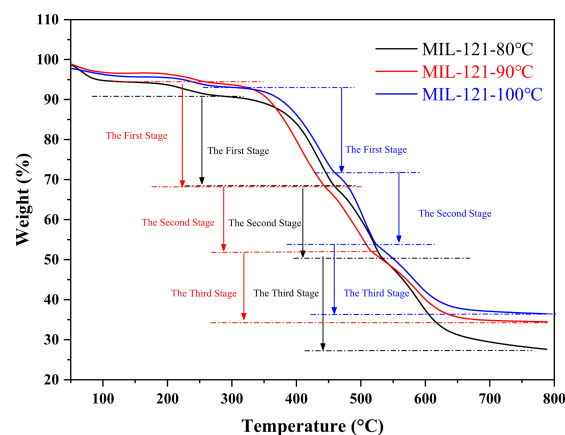


Figure 3. TG curves of MIL-121-80 °C, MIL-121-90 °C, MIL-121-100 °C.

3.2. Prediction of Crystal Morphology

The theoretical growth habit of MIL-121 was simulated using the Morphology module in Material studio. The unit cell data provided by the crystallographic information file [42]

are used to simulate the crystal morphology with BFDH model. The crystal morphology simulated with BFDH model is a regular polyhedron (Figure 4). According to the theoretical prediction, the addition of sodium hydroxide promoted the growth of $(\bar{2}00)$, $(1\bar{1}0)$, $(\bar{1}\bar{1}0)$, and (200) crystal planes. The accelerated growth rate of these crystal planes leads to a polyhedral morphology. In addition, the addition of sodium hydroxide generated higher supersaturation. Hence, the driving force for crystal nucleation and growth enhanced, which accelerated the nucleation rate and growth rate of MIL-121. The crystal morphologies of the real products are slightly different. The number and relative percentage of the exposed facets are shown in Table 1.

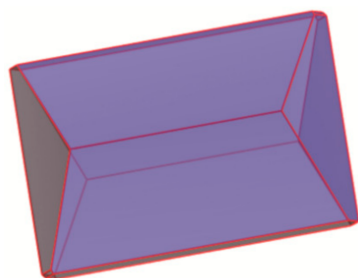


Figure 4. Crystal morphology of MIL-121 predicted by BFDH module.

Table 1. Crystal surface parameters of MIL-121.

Hkl	Dhkl/Å	Distance/Å	% Total Facet Area
{110}	10.39	9.63	63.43
{200}	8.06	12.40	10.01
{11 $\bar{1}$ }	5.98	16.72	26.37
{31 $\bar{1}$ }	4.84	20.68	0.19

3.3. Crystallization Process Promoted by NaOH

The droplets from the experiments, in Section 2.5, of the sample were naturally volatilized and crystallized in the fume hood and analyzed by Raman as shown in Figure 5. Figure 5a shows the Raman spectra of the blank sample without the addition of NaOH. The characteristic peaks of the in-plane symmetric stretching vibration of the nitrate radicals of $\text{Al}(\text{NO}_3)_3 \cdot 9\text{H}_2\text{O}$ are between 1035 and 1075 cm^{-1} , and the characteristic peaks of the benzene ring of H_4BTEC are at 1624 , 3092 cm^{-1} (the Raman peak analysis details of $\text{Al}(\text{NO}_3)_3 \cdot 9\text{H}_2\text{O}$, H_4BTEC , pyromellitic acid hydrate, and MIL-121 are shown in Figure S5, (Supplementary Materials)). The Raman peak analysis results of the intermediate sampling showed that the coordination reaction occurred when the metal salt and the ligand were dissolved in water. The Raman characteristic peak at $1035\sim 1075 \text{ cm}^{-1}$ was caused by the residual nitrate. It disappeared after washing.

Figure 5b shows the Raman analysis of samples taken during the process of adding sodium hydroxide to promote cooling and crystallization. The Raman characteristic peak at 762 cm^{-1} indicates pyromellitic acid hydrate before adding sodium hydroxide (the green dotted circle). After the dropwise addition of sodium hydroxide, the Raman characteristic peaks of the benzene ring and carboxyl group at 1169 , 1257 , and 1311 cm^{-1} disappeared (the black dashed box). This is because sodium hydroxide acts as a promoter to accelerate the conversion of homo benzene. NaOH captures metal ions and promotes the bonding of Al-O bonds. The characteristic peaks of MIL-121 at 798 , 812 , 825 cm^{-1} (the red circle) appeared in the product after adding sodium hydroxide for 5 h. Figure 5a shows the results of intermittent sampling and monitoring of the blank control group. The characteristic peak of MIL-121 did not appear until the end of the cooling crystallization process. This confirmed that sodium hydroxide promoted the production of MIL-121. It was also confirmed that a small amount of MIL-121 was contained in the sampled droplet crystal product after adding sodium hydroxide for 5 h.

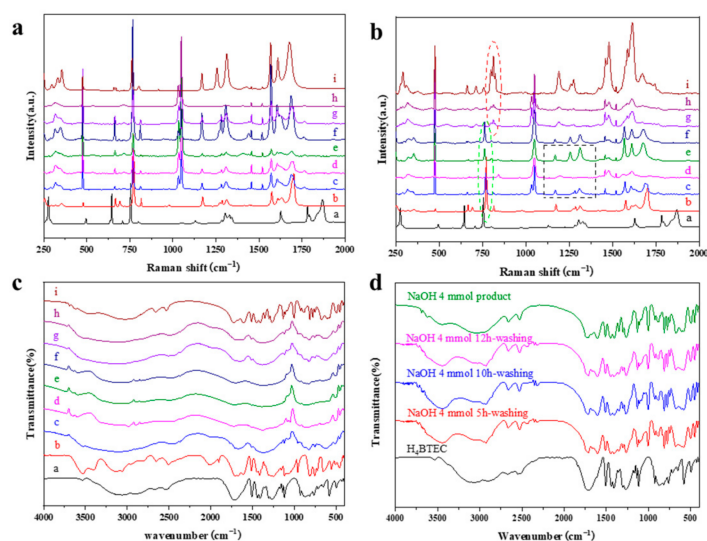


Figure 5. (a) Raman spectra of group A without NaOH. a, H₄BTEC; b, pyromellitic acid hydrate, c, initial saturated solution, d, after dissolution; e, refer stirring for 1 h; f, refer stirring for 3 h, g, refer stirring for 5 h, h, refer stirring for 10 h, i, refer stirring for 12 h. (b) Raman spectra of group B cooling crystallization process monitored. a, H₄BTEC; b, pyromellitic acid hydrate, c, initial saturated solution, d, before adding NaOH; e, refer adding NaOH for 1 h, f, refer adding NaOH for 3 h; g, refer adding NaOH for 5 h, h, refer adding NaOH for 10 h, i, refer adding NaOH for 12 h. (c) FTIR of group B cooling crystallization process monitored. a, H₄BTEC; b, pyromellitic acid hydrate; c, initial saturated solution, d, before adding NaOH; e, refer adding NaOH for 1 h, f, refer adding NaOH for 3 h, g, refer adding NaOH for 5 h, h, refer adding NaOH for 10 h, i, refer adding NaOH for 12 h. (d) FTIR of the sample after washing with ethanol.

The droplet crystallization product was further analyzed by FTIR, as shown in Figure 5c. The infrared peaks of the products sampled after adding sodium hydroxide for 3 and 5 h are consistent. Similarly, adding sodium hydroxide for 10 h and sodium hydroxide for 12 h showed the same peaks. In order to eliminate the influence of nitrate and pyromellitic acid and its hydrates, ethanol and water are used to clean the crystalline products of the naturally volatilized droplets. During the washing process, some samples were completely dissolved and a small amount of samples remained. The remained samples were dried in an oven at 80 °C and analyzed by Fourier infrared spectroscopy. Figure 5d shows the comparison between the infrared peaks of the sample after cleaning and the peaks of the raw material pyromellitic acid and the product MIL-121. The results confirmed that the infrared peaks of the sample after cleaning are consistent with those of MIL-121. Combined with the analysis of Raman spectroscopy, it was determined that the natural volatile crystalline product of droplets was a mixture of pyromellitic acid and its hydrate and MIL-121. Trace amounts of MIL-121 nuclei were formed after adding sodium hydroxide for 3 h. It was also determined that the optimal equilibrium time range for the preparation of MIL-121 by adding sodium hydroxide under ambient pressure was 5–10 h.

3.4. Optimization of Synthesis Parameters

A parallel crystallizer was used to carry out the optimization experiments under different reaction temperatures, reaction time, cooling rates, and the addition amount of NaOH. The experimental results were consistent with the conclusions drawn from the process investigation of preparing MIL-121 promoted by sodium hydroxide. That is, the optimal addition amount of NaOH is 1 mL aqueous solution with concentration of 4 mol/L, at a temperature of 80 °C, and the preparation time range is 5–10 h. Crystallization with the optimal operation parameters was carried out, and the product yield was higher and the morphology of the products was shown to be more uniform. On the contrary, extending the reaction time did not increase the product yield much, but both energy and time consump-

tion were prolonged. In addition, as the reaction temperature increases, the equilibrium time is significantly shortened and the yield becomes larger. However, the particle size of the product remains unchanged under normal pressure. Taken together, the cooling crystallization method proposed in this article can make it possible to prepare MIL-121 at atmospheric pressure with reaction time of several hours. Considering the comprehensive factors such as product yield, the reaction time can be shortened to 5–10 h when the reaction temperature was 80 °C. When the reaction temperature approached 100 °C, the preparation time can be shortened to be less than 5 h. This method greatly decreased the preparation cost and time, and the preparation conditions were relatively mild. MIL-121 with uniform particle size distribution can be obtained under ambient pressure and low temperature conditions (Table S3, Supplementary Materials, the preparation method and preparation time of common aluminum-based MOF.)

The morphology of the products collected in the cooling crystallization of MIL-121 promoted by the NaOH and the morphology of the products obtained in the large-scale experiment were both characterized by SEM as shown in Figure 6. The morphology of MIL-121 obtained by cooling crystallization was consistent with the morphology of the products collected by the hydrothermal method. They were both regular polyhedron. The difference was that the products obtained by cooling crystallization were attached with smaller particles of MIL-121. The particle size distribution diagram of large-scale experimental product was shown in Figure S4d (Supplementary Materials). The particle size distribution is more uniform than that of hydrothermal synthesis products. The particle size of the cooling crystallization product was smaller than that of the hydrothermal method at the same temperature, and the median diameter D50 is 1.57 μm . The stability of the product was confirmed by TG. The derivative in Figure 7 demonstrated that the sample decomposed step-by-step as the temperature increases. The first stage is mainly the removal of the solvent ethanol and deionized water used for cleaning, and the subsequent stage is the decomposition of the carboxyl group and the framework. The dehydration temperature is 246 °C, and the initial decomposition temperature is about 386 °C. Compared with the thermal stability data of the hydrothermal method MIL-121-80 °C, MIL-121-90 °C, and MIL-121-100 °C products (Table S4, Supplementary Materials), the thermal stability of the product produced by cooling crystallization is better.

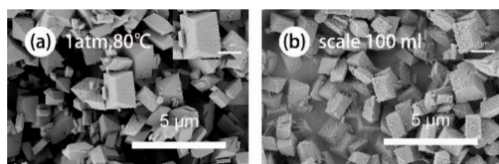


Figure 6. SEM images of (a) MIL-121-1 atm, 80 °C, (b) MIL-121-scale 100 mL.

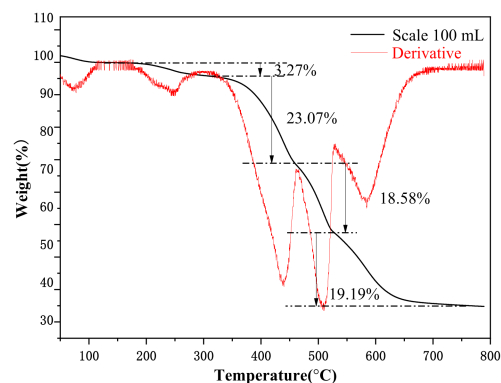


Figure 7. TG curves of MIL-121-scale 100 mL.

On the basis of the 100 mL scale cooling crystallization experiment, a 250 mL crystallizer was used for scale-up experiments. The results of the scale-up experiment were

similar to those of the scale 100 mL experiment. The preparation method can quickly prepare MIL-121 with high thermal stability under ambient pressure, and potentially pave the way for the industrial production of MIL-121.

3.5. Lithium Ion Adsorption Performance

The MIL-121 prepared at three different synthesis temperatures and two different scales were polymerized by introducing DMVBA (*N,N*-dimethyl-vinyl-benzyl-amine) monomer into the pores of MIL-121 by the solution radical polymerization method. MIL-121 is functionalized, making it a composite material PDMVBA-MIL-121 [18] with both free carboxyl groups and amine groups with adsorption properties. A histogram was made according to the adsorption capacity (Table S5, Supplementary Materials) as shown in Figure 8. It can be clearly seen that MIL-121 prepared at three different synthesis temperatures and two different scales has little difference in the adsorption performance of lithium ions after polymerization modification, and the adsorption capacity is basically the same at about 0.18 mmol/g. That is, the small particle size MIL-121 prepared by the hydrothermal method and the MIL-121 prepared by the cooling crystallization method have the same adsorption performance for lithium ions after the polymerization modification. However, compared with the hydrothermal method, the cooling crystallization method can quickly obtain a large amount of MIL-121 under ambient pressure, with better reproducibility and operability.

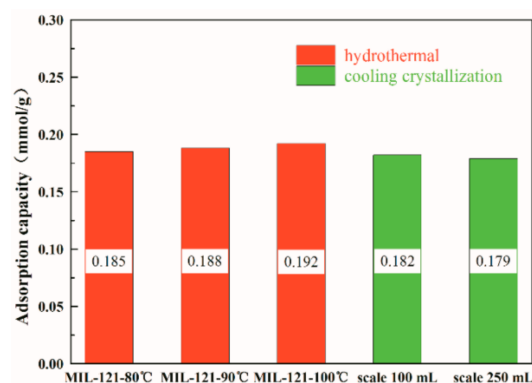


Figure 8. The adsorption performance diagram of MIL-121 obtained under different experimental conditions.

4. Conclusions

A novel method to generate MIL-121 under ambient pressure was developed. Sodium hydroxide was used as the promoter in the novel method to promote the coordination between metal ions and ligands of MIL-121 without the reaction condition of high temperature and pressure, so that MIL-121 can be produced under ambient pressure. The experimental result indicates that there is no difference in the lithium-ion adsorption performance between the products of MIL-121 obtained by the cooling crystallization method and hydrothermal method. However, compared with the hydrothermal method, the cooling crystallization method greatly shortens the preparation time and production cost of MIL-121. In this paper, the optimal synthesis strategy of the cooling crystallization method was also determined and a small-scale cooling crystallization experiment was carried out under the guidance of the optimal synthesis strategy. The MIL-121 products obtained by this method are of a uniform size and higher stability compared with the products prepared by the hydrothermal reaction at the same temperature. The alkali-assisted mechanism of this method was estimated, and effect of reaction condition on the morphology and crystal size of MIL-121 crystal products was investigated. The experimental results demonstrate that the MIL-121 can be produced by the traditional cooling crystallization without high temperature and pressure, which provided a basis for the industrialization of aluminum-based MOF (MIL-121).

Supplementary Materials: The following are available online at <https://www.mdpi.com/article/10.3390/coatings11070854/s1>. Figure S1: SEM images of products under different sodium hydroxide addition conditions, Figure S2: (a) Raman diagram of products with different sodium hydroxide addition levels, (b) Centrifugation results of products with addition volume of 16 mmol, Figure S3: (a) FTIR spectrum of MIL-121 and (b) Raman spectrum of MIL-121, Figure S4: Size distribution of (a) MIL-121-80 °C (hydrothermal method from Section 2.4), (b) MIL-121-90 °C (hydrothermal method from Section 2.4), (c) MIL-121-100 °C (hydrothermal method from Section 2.4), (d) MIL-121-80 °C scale 100 mL (Cooling crystallization method from Section 2.6), Figure S5: Raman spectra of (a) $\text{Al}(\text{NO}_3)_3 \cdot 9\text{H}_2\text{O}$, (b) H_4BTEC , (c) pyromellitic acid hydrate, (d) MIL-121, Figure S6: (a) PXRD pattern of MIL-121-(1 atm, 80 °C), EasyMax product, (b) FTIR spectrum of MIL-121-(1 atm, 80 °C), EasyMax product and (c) Raman spectrum of MIL-121-(1 atm, 80 °C), EasyMax product, Table S1: Peaks location of PXRD pattern and the crystal indices of MIL-121 [2], MIL-121-80 °C NaOH 4 mmol, Table S2: The particle size distribution of MIL-121 under different temperature, Table S3: Preparation method and preparation time of partial aluminum-based MOF, Table S4: TGA mass loss of N-MIL-121 crystals synthesized under different conditions, Table S5: The adsorption performance test data of MIL-121 after polymerization obtained under different experimental condition.

Author Contributions: Writing—review and editing, investigation and validation, Q.W., S.S. and B.S.; formal analysis and writing—original draft preparation, F.W.; writing—review and editing, and supervision, L.Z. and X.Z. All authors have read and agreed to the published version of the manuscript.

Funding: Natural Science Foundation of Tianjin Municipality (18JCYBJC21200).

Institutional Review Board Statement: Not applicable.

Informed Consent Statement: Not applicable.

Data Availability Statement: Data is contained within Supplementary Materials. The data presented in this study are available in Supplementary Materials.

Acknowledgments: Thanks to the College of Chemical Engineering and Materials Science for providing instruments and experimental materials.

Conflicts of Interest: The authors declare no conflict of interest.

References

1. Swain, B. Recovery and recycling of lithium: A review. *Sep. Purif. Technol.* **2017**, *172*, 388–403. [[CrossRef](#)]
2. Jiang, H.; Yang, Y.; Sun, S.; Yu, J. Adsorption of lithium ions on lithium-aluminum hydroxides: Equilibrium and kinetics. *Can. J. Chem. Eng.* **2020**, *98*, 544–555. [[CrossRef](#)]
3. Chung, K.; Lee, J.; Kim, W.; Kim, S.; Cho, K. Inorganic adsorbent containing polymeric membrane reservoir for the recovery of lithium from seawater. *J. Membr. Sci.* **2008**, *325*, 503–508. [[CrossRef](#)]
4. Zhang, Y.; Hu, Y.; Wang, L.; Sun, W. Systematic review of lithium extraction from salt-lake brines via precipitation approaches. *Miner. Eng.* **2019**, *139*, 105868. [[CrossRef](#)]
5. Zhao, X.; Yang, H.; Wang, Y.; Sha, Z. Review on the electrochemical extraction of lithium from seawater/brine. *J. Electroanal. Chem.* **2019**, *850*, 113389. [[CrossRef](#)]
6. Zhao, X.; Li, G.; Feng, M.; Wang, Y. Semi-continuous electrochemical extraction of lithium from brine using CF-NMMO/AC asymmetric hybrid capacitors. *Electrochim. Acta* **2019**, *331*, 135285. [[CrossRef](#)]
7. Zhao, X.; Jiao, Y.; Xue, P.; Feng, M.; Sha, Z. Efficiently lithium extraction from brine by using three-dimensional (3D) nanostructured hybrid inorganic-gel framework electrode. *ACS Sustain. Chem. Eng.* **2020**, *8*, 4827–4837. [[CrossRef](#)]
8. Zhao, X.; Feng, M.; Jiao, Y.; Zhang, Y.; Wang, Y.; Sha, Z. Lithium extraction from brine in an ionic selective desalination battery. *Desalination* **2020**, *481*, 114360. [[CrossRef](#)]
9. Hu, S.; Sun, Y.; Pu, M.; Yun, R.; Xiang, X. Determination of boundary conditions for highly efficient separation of magnesium and lithium from salt lake brine by reaction-coupled separation technology. *Sep. Purif. Technol.* **2019**, *229*, 115813. [[CrossRef](#)]
10. Liu, Y.T.; Chen, T.-Y.; Wang, M.K.; Huang, P.M.; Chiang, P.-N.; Lee, J.F. Mechanistic study of arsenate adsorption on lithium/aluminum layered double hydroxide. *Appl. Clay Sci.* **2010**, *48*, 485–491. [[CrossRef](#)]
11. Shi, C.; Jing, Y.; Jia, Y. Solvent extraction of lithium ions by tri-n-butyl phosphate using a room temperature ionic liquid. *J. Mol. Liq.* **2016**, *215*, 640–646. [[CrossRef](#)]
12. Wei, X.; Liang, S.; Zhou, Z.; Qin, W.; Fei, W. Extraction of lithium from salt lake brine containing borate anion and high concentration of magnesium. *Hydrometallurgy* **2016**, *166*, 9–15.
13. Tian, L.; Wei, M.; Mei, H. Adsorption behavior of Li^+ onto nano-lithium ion sieve from hybrid magnesium/lithium manganese oxide-sciencedirect. *CEJ* **2010**, *156*, 134–140.

14. Kotsupalo, N.; Ryabtsev, A. Effect of structure on the sorption properties of chlorine-containing form of double aluminum lithium hydroxide. *Russ. J. Appl. Chem.* **2013**, *86*, 482–487. [[CrossRef](#)]
15. Nisola, G.M.; Limjuco, L.A.; Vivas, E.L.; Lawagon, C.P.; Park, M.J.; Shon, H.K.; Mittala, N.; Nah, I.W.; Kim, H.; Chung, W. Macroporous flexible polyvinyl alcohol lithium adsorbent foam composite prepared via surfactant blending and cryo-desiccation. *CEJ* **2015**, *280*, 536–548. [[CrossRef](#)]
16. Chitrakar, R.; Makita, Y.; Ooi, K.; Sonoda, A. Magnesium-doped manganese oxide with lithium ion-sieve property: Lithium adsorption from salt lake brine. *Bull. Chem. Soc. Jpn.* **2013**, *86*, 850–855. [[CrossRef](#)]
17. Bi, Q.; Zhang, Z.; Zhao, C.; Tao, Z. Study on the recovery of lithium from high Mg^{2+}/Li^{+} ratio brine by nanofiltration. *Water Sci. Technol.* **2014**, *70*, 1690–1694. [[CrossRef](#)]
18. Ou, R.; Zhang, H.; Wei, J.; Kim, S.; Wan, L.; Nguyen, N.S.; Hu, Y.; Zhang, X.; Simon, G.P. Thermoresponsive amphoteric metal-organic frameworks for efficient and reversible adsorption of multiple salts from water. *Adv. Mater.* **2018**, *30*, e1802767. [[CrossRef](#)]
19. Ji, C.; Wu, D.; Lu, J.; Shan, C.; Ren, Y.; Li, T.; Lv, L.; Pan, B.; Zhang, W. Temperature regulated adsorption and desorption of heavy metals to a-Mil-121: Mechanisms and the role of exchangeable protons. *Water Res.* **2020**, *189*, 116599. [[CrossRef](#)]
20. Yamamoto, D.; Maki, T.; Watanabe, S.; Tanaka, H.; Miyahara, M.T.; Mae, K. Synthesis and adsorption properties of zif-8 nanoparticles using a micromixer. *CEJ* **2013**, *227*, 145–150.
21. Marshall, C.; Staudhammer, S.A.; Brozek, C.K. Size control over metal-organic framework porous nanocrystals. *Chem. Sci.* **2019**, *10*, 9396–9408. [[CrossRef](#)]
22. Han, Y.-H.; Tian, C.-B.; Li, Q.-H.; Du, S.-W. Highly chemical and thermally stable luminescent EuxTb1-xMOF materials for broad-range pH and temperature sensors. *J. Mater. Chem. C* **2014**, *2*, 8065–8070. [[CrossRef](#)]
23. Mendiratta, S.; Usman, M.; Chang, C.; Lee, Y.C.; Chen, J.W.; Wu, M.K. Zn(ii)-based metal-organic framework: An exceptionally thermally stable, guest-free low dielectric material. *J. Mater. Chem.* **2017**, *5*, 1508–1513. [[CrossRef](#)]
24. Kamal, S.; Chiou, K.R.; Sainbileg, B.; Inamdar, A.I.; Usman, M.; Pathak, A.; Luo, T.-T.; Chen, J.-W.; Hayashi, M.; Hung, C.-H.; et al. Thermally stable indium based metal-organic frameworks with high dielectric permittivity. *J. Mater. Chem. C* **2020**, *8*, 9724–9733. [[CrossRef](#)]
25. Zhu, Y.P.; Yin, J.E.; Abou-Hamad, X.; Liu, W.; Chen, T. Highly stable phosphonate-based mofs with engineered bandgaps for efficient photocatalytic hydrogen production. *Adv. Mater.* **2020**, *32*, 1906368. [[CrossRef](#)]
26. Ricco, R.; Liang, W.; Li, S.; Gassensmith, J.J.; Caruso, F.; Doonan, C.; Falcaro, P. Metal-organic frameworks for cell and virus biology: A perspective. *ACS Nano* **2018**, *12*, 13–23. [[CrossRef](#)]
27. Li, H.; Lv, N.; Li, X.; Liu, B.; Feng, J.; Ren, X.; Guo, T.; Chen, D.; Stoddart, J.F.; Gref, R.; et al. Composite CD-MOF nanocrystals-containing microspheres for sustained drug delivery. *Nanoscale* **2017**, *9*, 7454–7463. [[CrossRef](#)]
28. Li, S.; Huo, F. Metal-organic framework composites: From fundamentals to applications. *Nanoscale* **2015**, *7*, 7482–7501. [[CrossRef](#)]
29. Liu, M.; Xie, K.; Nothling, M.D.; Gurr, P.A.; Tan, S.S.L.; Fu, Q.; Webley, P.A.; Qiao, G.G. Ultrathin metal-organic framework nanosheets as a gutter layer for flexible composite gas separation membranes. *ACS Nano* **2018**, *12*, 11591–11599. [[CrossRef](#)]
30. Stavila, V.; Bhakta, R.K.; Alam, T.M.; Majzoub, E.H.; Allendorf, M.D. Reversible hydrogen storage by NaAlH₄ confined within a titanium-functionalized MOF-74(Mg) nanoreactor. *ACS Nano* **2012**, *6*, 9807–9817. [[CrossRef](#)]
31. Babal, A.S.; Tan, J.-C. Influence of mechanical, thermal, and electrical perturbations on the dielectric behaviour of guest-encapsulated HKUST-1 crystals. *J. Mater. Chem. C* **2020**, *8*, 12886–12892. [[CrossRef](#)]
32. Bi, S.; Banda, H.; Chen, M.; Niu, L.; Chen, M.; Wu, T.; Wang, J.; Wang, R.; Feng, J.; Chen, T.; et al. Molecular understanding of charge storage and charging dynamics in supercapacitors with Mof electrodes and ionic liquid electrolytes. *Nat. Mater.* **2019**, *19*, 552–558. [[CrossRef](#)]
33. Van Vleet, M.; Weng, T.; Li, X.; Schmidt, J. In situ, time-resolved, and mechanistic studies of metal-organic framework nucleation and growth. *Chem. Rev.* **2018**, *118*, 3681–3721. [[CrossRef](#)]
34. Chen, J.; Shen, K.; Li, Y. Greening the processes of metal-organic framework synthesis and their use in sustainable catalysis. *ChemSusChem* **2017**, *10*, 3165–3187. [[CrossRef](#)]
35. Ibarra, I.A.; Bayliss, P.A.; Yang, S.; Nowell, H.; Poliakov, M.; Pérez, E.; Blake, A.J.; Allan, D.R.; Schröder, M. Near-critical water, a cleaner solvent for the synthesis of a metal-organic framework. *Green Chem.* **2012**, *14*, 117–122. [[CrossRef](#)]
36. Guo, W.; Sun, W.; Lv, L.P.; Kong, S.; Wang, Y. Microwave-assisted morphology evolution of Fe-based metal-organic frameworks and their derived Fe₂O₃ nanostructures for Li-ion storage. *ACS Nano* **2017**, *11*, 4198–4205. [[CrossRef](#)] [[PubMed](#)]
37. Li, Z.Q.; Qiu, L.G.; Tao, X.; Yun, W.; Wei, W.; Wu, Z.Y. Ultrasonic synthesis of the microporous metal-organic framework Cu₃(btc)₂ at ambient temperature and pressure: An efficient and environmentally friendly method. *Mater. Lett.* **2019**, *63*, 78–80. [[CrossRef](#)]
38. Yan, D.; Gao, R.; Wei, M.; Li, S.; Lu, J.; Evans, D.G.; Duan, X. Mechanochemical synthesis of a fluorenone-based metal organic framework with polarized fluorescence: An experimental and computational study. *J. Mater. Chem. C* **2013**, *1*, 997–1004. [[CrossRef](#)]
39. Friščić, T.; Halasz, I.; Štrukil, V.; Eckert-Maksić, M.; Dinnebier, R.E. Clean and efficient synthesis using mechanochemistry: Coordination polymers, metal-organic frameworks and metallodrugs. *Croat. Chem. Acta* **2012**, *85*, 367–378. [[CrossRef](#)]
40. Gaab, M.; Trukhan, N.; Maurer, S.; Gummaraju, R.; Müller, U. The progression of Al-based metal-organic frameworks—From academic research to industrial production and applications. *Microporous Mesoporous Mater.* **2012**, *157*, 131–136. [[CrossRef](#)]

41. Wang, F.; Zhu, L.; Wei, Q.Y.; Wang, Y.F. Research on the effects of hydrothermal synthesis conditions on the crystal Hab-it of Mil-121. *R. Soc. Open Sci.* **2020**, *7*, 201212. [[CrossRef](#)] [[PubMed](#)]
42. Volkringer, C.; Loiseau, T.; Guillou, N.; Férey, G.; Haouas, M.; Taulelle, F.; Elkaim, E.; Stock, N. High-throughput aided synthesis of the porous metal–organic framework-type aluminum pyromellitate, MIL-121, with extra carboxylic acid functionalization. *Inorg. Chem.* **2010**, *49*, 9852–9862. [[CrossRef](#)] [[PubMed](#)]